Investigation of SARS-CoV-2 nucleocapsid protein interaction with a specific antibody by combined spectroscopic ellipsometry and quartz crystal microbalance with dissipation

Ieva Plikusiene [a], Vincentas Maciulis [a,b], Silvija Juciute [a], Arunas Ramanavicius [a], Zigmas Balevicius [b], Rimantas Slibinskas [c], Indre Kucinskaite-Kodze [c], Martynas Simanavicius [c], Saulius Balevicius [a,b], Almira Ramanaviciene [a,*]

[a] NanoTechnas – Center of Nanotechnology and Materials Science, Faculty of Chemistry and Geosciences, Vilnius University, Naugarduko str. 24, 03225 Vilnius, Lithuania
[b] State Research Institute Center for Physical Sciences and Technology, Sauletekio ave. 3, Vilnius, Lithuania
[c] Institute of Biotechnology, Life Sciences Center, Vilnius University, Sauletekio ave. 7, LT-10257 Vilnius, Lithuania

GRAPHICAL ABSTRACT
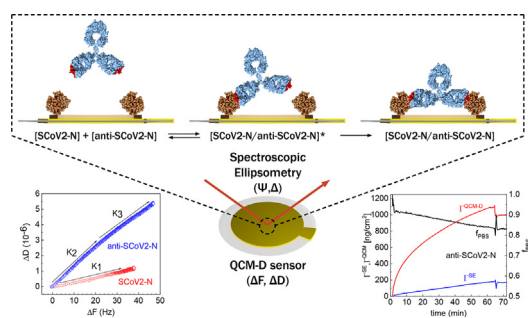
ARTICLE INFO

ABSTRACT

Detailed evaluations of the antigen and antibody interaction rate and strength of the immune complex formed are very important for medical and bioanalytical applications. These data are crucial for the development of sensitive and fast immunosensors suitable for continuous measurements. Therefore, combined spectroscopic ellipsometry (SE) and quartz crystal microbalance with dissipation (QCM-D) technique (SE/QCM-D) was used for the evaluation: (i) of covalent immobilization of SARS-CoV-2 nucleocapsid protein (SCoV2-N) on QCM-D sensor disc modified by self-assembled monolayer based on 11-mercaptoundecanoic acid and (ii) interaction of immobilized SCoV2-N with specific polyclonal anti-SCoV2-N antibodies followed by immune complex formation process. The results show that the SCoV2-N monolayer is rigid due to the low energy dissipation registered during the QCM-D measurement. In contrast, the anti-SCoV2-N layer produced after interaction with the immobilized SCoV2-N formed a soft and viscous layer. It was determined, that the sparse distribution of SCoV2-N on the surface affected the spatial arrangement of the antibody during the formation of immune complexes. The hinge-mediated flexibility of the antibody Fab fragments allows them to reach the more distantly located SCoV2-N and establish a bivalent binding between proteins in the formed SCoV2-N/anti-SCoV2-N complex. It was noted that the SE/QCM-D method can provide more precise quantitative information about the flexibility and conformational changes of antibody during the formation of the immune complex on the surface over time.

© 2022 Elsevier Inc. All rights reserved.

* Corresponding author.
  E-mail address: almira.ramanaviciene@chf.vu.lt (A. Ramanaviciene).

1. Introduction

The health challenges associated with the rapid spread of Severe Acute Respiratory Syndrome Coronavirus 2 (SARS-CoV-2) have recently led to intensive studies of the SARS-CoV-2 nucleocapsid protein (SCoV2-N) and specific polyclonal antibodies (anti-SCoV2-N). Although the main focus of research has been on the SARS-CoV-2 spike protein, the investigations of the nucleocapsid protein are also important due to their critical impact on the coronavirus genomic RNR packing and viral replication [1]. Immunoglobulin G (IgG) antibodies against the SARS-CoV-2 nucleocapsid protein are detectable in infected patients. A higher titer of these antibodies was determined to be a prognostic factor of the clinical course of disease [2]. Therefore, more information on such antibody interaction with the SARS-CoV-2 nucleocapsid protein is needed. During the pandemic, different methods were developed for the detection of SARS-CoV-2 and the diagnosis of COVID-19 infection, including different serological tests to record antibody (Ab) and antigen (Ag) interactions [3,4]. Usually, as a result of the test, Abs against the most immunogenic SARS-CoV-2 spike protein and/or nucleocapsid protein are detected [5,6]. Furthermore, it was determined that Abs to the nucleocapsid protein are more sensitive to the diagnosis of early infection than Abs specific to the spike protein [7]. For this reason, the research that helps to understand how SARS-CoV-2 nucleocapsid protein interact with specific anti-SCoV2-N Abs is very expected for the industry involved in the production of viral proteins, Ab-Ag tests, and vaccines.

It is well known that Abs are large globular Y-shaped glycoproteins consisting of two heavy and two light chains. Two pairs of light and heavy chains are connected by disulfide bonds, and two heavy chains are connected by disulfide bonds located in the hinge region. This region is a flexible tether present in the IgG, IgA and IgD class Abs, and responsible for the movement of two Ab Fab fragments (antibody regions corresponding to antigen-binding fragments and consisting of both the variable and constant regions of heavy and light chains) and changes in Fab-Fab angles. IgG class Abs are the most abundant class of Abs in the blood produced by the organism after contact with the antigen. The impact of different human IgG subclass hinge-mediated flexibility on the type and sizes of soluble immune complexes was analyzed by electron microscopy. The IgG subclasses, depending on their flexibility, were ranked in such an order (most to least flexible): IgG3 > IgG1 > IgG4 > IgG2; accordingly, the mean angles between Fab-Fab were determined as 136°, 128°, 127°, and 117° [8]. The hinge-mediated flexibility of Abs, the wagging and rotational movements of the Fab fragments, the steric interactions of two Fab fragments with each other and with crystallizable fragment (Fc) of Ab are significant for the binding of Ab to Ag of different size, from small haptens to relatively large viruses [9]. The Ab affinity is defined as the combined strength of a single Ab antigen-binding site interaction with a single epitope present in the Ag structure. The Ab avidity (IgG class) is defined as the total strength of all noncovalent bivalent (Fab-Fab) affinity interactions with two epitopes. It was determined that the bivalent binding of monoclonal Abs to human immunodeficiency virus type 1 envelope glycoprotein trimer 2F5 epitopes results in greatly enhanced neutralization efficiency through an increase in binding avidity [10]. Additionally, the impact of CD20 epitopes surface density on the recognition and bivalent interaction with monoclonal Abs (rituximab) was analyzed using quartz crystal microbalance with dissipation (QCM-D) and surface plasmon resonance (SPR) technique [11]. To study the affinity and avidity features of the anti-SCoV2-N, the noncontact, real time and sensitive methods are required. Among them very promising is the polarization sensitive optical method named as spectroscopic ellipsometry (SE) and sur-

face mass sensitive QCM-D technique method, which is based on the assessment of surface acoustic wave dissipation.

The SE is a nondestructive, label-free and highly sensitive optical technique that allows to determine the refractive index n or the thicknesses d of the formed protein layers [12–15]. These values can be used to calculate the dry surface mass of the protein layer [16–18]. During the ellipsometric measurement, two ellipsometric parameters are determined – Ψ that corresponds to the light wave amplitude and Δ that gives the information of the light phase shift after reflection from the sample. To enhance the sensitivity of the SE method, it is applied in the total internal reflection mode (TIRE) [16,19–23]. However, the SE method is not able to measure n and d values separately. Therefore, regression analysis is used to calculate the n and d values, which requires specific information about the geometry and refractive index of the proteins. The certain inaccuracy of the n and d determination from the regression analysis depends on the knowledge about these parameters.

QCM-D measures the shifts in frequency (ΔF) and energy dissipation (ΔD) of vibrational resonance overtones. It enables to determine the surface mass coupled to a pre-modified quartz crystal sensor and viscoelastic properties of the layer [12,24,25]. The mass obtained from QCM-D measurements refers to the wet mass when it is obtained for the layer of proteins coupled to the surface together with the buffer. In the case of very strong coupling (low ΔD values) between antibodies and immobilized proteins, the shifts in frequency (ΔF) of the QCM-D method give unambiguous information about the mass on the sensing surface. However, this assumption is usually not fully satisfied. Thus, for the determination of immobilized proteins layer mass and viscoelastic properties it is necessary to make several assumptions concerning models of continuum mechanics [26].

In both SE and QCM-D methods, the response signal depends on the immobilized protein mass; however, SE gives additional information about the dielectric properties of proteins layers, while QCM-D provides information about the viscoelastic properties. Thus by combining SE and QCM-D, it is possible to derive the solvent content of thin protein layers formed on the surface [24,27] and using regression analysis to obtain more precise information about antibody avidity properties. That leads to better understanding of protein–protein interaction mechanism and changes of protein conformation after specific interaction. The hybrid SE/QCM-D method could reveal additional new possibilities for antigen–antibody interaction and analysis of immune complex formation, providing quantitative information that cannot be obtained when the SE and QCM-D methods are used separately [28].

The affinity properties of the SARS-CoV-2 nucleocapsid protein (SCoV2-N) and specific anti-SCoV2-N antibodies were analyzed using the SE method in our previous work [29]. Now, we have used the hybrid SE/QCM-D technique to investigate (i) the covalent immobilization of SCoV2-N on the 11-mercaptoundecanoic acid (11-MUA) self-assembled monolayer (SAM) modified QCM-D gold sensor and (ii) the interaction with specific antibodies followed by an immune complex formation process to evaluate the structural and viscoelastic properties of the layers formed.

2. Materials and methods

2.1. Materials

11-Mercaptoundecanoic acid (11-MUA, 98%), N-(3-diemethylaminopropyl)-N'-ethylcarbodiimide hydrochloride ($\geq$98%) (EDC), *N*-Hydroxysuccinimide (98%) (NHS), sodium hydroxide ($\geq$97%), ethanolamine (ETA) ($\geq$99%), sodium dodecyl sulfate ($\geq$99%) (SDS) and phosphate buffered saline (PBS) tablets were purchased from Sigma Aldrich. Methanol (99.9%), ammonium sulfate ($\geq$99%), and

hexane (99%) were purchased from Carl Roth GmbH & Co (Karlsruhe, Germany). SARS-CoV-2 recombinant nucleoprotein (SCoV2-N) (≥97%) was received from Baltymas (Vilnius, Lithuania) [29]. QCM-D gold sensors were purchased from Biolin Scientific (Gothenburg, Sweden). Specific polyclonal antibodies (anti-SCoV2-N) obtained from immunized mice and nonspecific polyclonal antibodies obtained from non-immunized mice used in this work were developed under the procedure in detail described in our previous work [29]. Anti-SCoV2-N antibodies were purified from blood serum by ammonium sulfate precipitation, which results in 90% purity. All experiments using laboratory mice were performed under controlled laboratory conditions according to European and Lithuanian legislation (permission no. G2-117 issued by the State Food and Veterinary Service, Vilnius, Lithuania).

2.2. The combined SE/QCM-D measurement setup

A combined SE/QCM-D measurement setup consists of SE and QCM-D techniques. QCM-D QSense Explorer, operating at frequency range 5 MHz, that allows the measurement of 7 harmonics and full viscoelastic modelling (Biolin Scientific, Sweden, with proprietary software QSoft401) was connected with a spectroscopic ellipsometry module, mounted on a rotating compensator spectroscopic ellipsometer M-2000X, operating in a spectral range from 200 nm to 1000 nm wavelength (J. A. Woolam, USA, with proprietary software for data analysis Complete EASE). Ellipsometric measurements were performed at a fixed 65° angle of incident light in a 200–1000 nm wavelength range. For the evaluation of the SCoV2-N and anti-SCoV2-N layers formed during the immobilization of SCoV2-N followed by the interaction with anti-SCoV2-N, the simulation of Δ and Ψ vs λ curves was performed using the Complete EASE software (Woollam, USA). Liquid flow was regulated with a peristaltic pump (Cole-Parmer GmbH, Germany) connected to a liquid intake through a flow chamber with PTFE tubing. The measurements were performed by injecting the liquids at a rate of 1.35 mL/min. During the measurements, the temperature inside the SE/QCM-D module was kept at 20 °C. The volume of the QSense Explorer chamber above the QCM-D gold sensor was 100 μl. QSoft401 software was used for the analysis of the frequency change (ΔF) and energy dissipation (ΔD) kinetics during covalent immobilization of SCoV2-N and affinity interaction with anti-SCoV2-N. The modelled values that can be obtained from such kinetics analysis are: the mass, thickness, and viscoelasticity of the formed protein layers.

2.3. Surface modification with 11-MUA

The QCM-D gold-coated sensor disc surface was prepared for modification with 11-MUA by cleaning in an ultrasonic bath, first in hexane and later in methanol for 2 min, respectively. The sensor surface was rinsed with methanol. A self-assembled monolayer (SAM) of 11-MUA was formed by immersing the QCM-D sensor disc into a solution of 1 mM of 11-MUA in methanol for 22 h. After-

wards, it was rinsed with methanol and dried with compressed air. A modified QCM-D sensor disc was placed and fixed in an SE/QCM-D module. Then the module chamber was filled with deionized water to establish a baseline for 30 min. For the activation of carboxyl groups of 11-MUA SAM, the solution of 0.1 M NHS and 0.4 M EDC mixed in equal parts was injected into the chamber for 15 min. Subsequently, deionized water was injected for the establishment of the baseline for 10 min.

2.4. Immobilization of SCoV2-N and deactivation of the activated carboxyl groups

In the next step of the experiment, SCoV2-N was covalently immobilized on the surface of the 11-MUA SAM modified QCM-D sensor disc. The PBS solution was injected into the chamber for 60 s and left stagnant for 10 min to establish a baseline. Subsequently, a 1.02 μM concentration SCoV2-N solution in PBS was pumped to the premodified QCM-D sensor disc and left to incubate for about 60 min. until a steady state conditions in both SE and QCM-D simultaneous measurements were achieved. Then, washing with PBS was performed for 10 min. Subsequently, the surface was treated with 1 M ethanolamine hydrochloride, pH 8.5, for 10 min to deactivate the remaining activated carboxyl groups. Then PBS was injected into the SE/QCM-D chamber for 20 min until steady state conditions were reached.

2.5. Formation of SCoV2-N/anti-SCoV2-N complex and regeneration of the surface for multiple detection of anti-SCoV2-N

The solution of 170 nM polyclonal anti-SCoV2-N antibody in PBS was injected into the chamber for 65 min for SCoV2-N/anti-SCoV2-N complex formation. The association phase was followed by the dissociation phase using PBS for 20 min. Afterwards, a regeneration solution consisting of 50 mM NaOH and 17.34 mM SDS was injected for 5 min, and the removal of anti-SCoV2-N from the surface was registered. Following, PBS solution was injected for 20 min to ensure that the remaining SCoV2-N layer is stable and not affected by the regeneration solution. Subsequently, the solution containing the same concentration (170 nM) of nonspecific antibodies was injected into the chamber for 30 min and washed with PBS. The schematic representation of the formation of the SCoV2-N/anti-SCoV2-N complex is presented in Fig. 1.

3. Results and discussion

Covalent SCoV2-N immobilization on 11-MUA SAM, and interaction with the anti-SCoV2-N kinetics were registered simultaneously using a combined setup of SE with QCM-D.
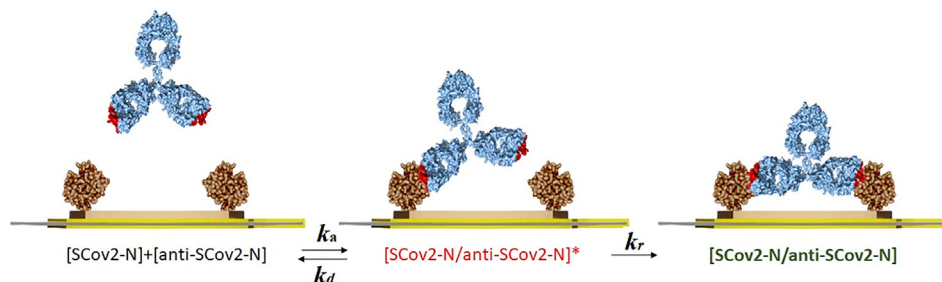

Fig. 1. Schematic representation of the anti-SCoV2-N interaction with covalently immobilized SCoV2-N. The formation of the immune complex takes two steps.

3.1. QCM-D-based assessment of SCoV2-N covalent immobilization and affinity interaction with anti-SCoV2-N

The changes in ΔF and ΔD by all overtones mastered by QCM-D were registered. The dependences of ΔF and ΔD vs. time for the third, fifth and seventh overtones are presented in Fig. 2. The information provided by the changes in ΔD corresponds to the viscoelastic properties of the formed SCoV2-N monolayer and SCoV2-N/anti-SCoV2-N complexes. As shown in Fig. 2, ΔD after covalent SCoV2-N immobilization is $1.09 \cdot 10^{-6}$ while after interaction with anti-SCoV2-N ΔD changed to $4.33 \cdot 10^{-6}$. The value of ΔD obtained after SCoV2-N immobilization on 11-MUA is small, therefore SCoV2-N layer can be considered as rigid and its properties can be described using the Sauerbrey equation [30,31].

ΔD measured for the anti-SCoV2-N interaction with SCoV2-N was 3.9 times higher than in the case of covalent SCoV2-N immobilization on 11-MUA self-assembled monolayer formed on the sensor disc. Anti-SCoV2-N monolayer viscoelastic properties were described using the Smart fit viscoelastic model from DFind software (Biolin). The decrease in frequency indicated an increase of surface mass density after covalent SCoV2-N immobilization and affinity interaction with anti-SCoV2-N. For SCoV2-N immobilization, ΔF was 37.63 Hz, while after interaction with anti-SCoV2-N during the same time interval, it was 47.57 Hz. Such changes of ΔF after SCoV2-N/anti-SCoV2-N complex formation confirmed the specific affinity interaction between SCoV2-N and anti-SCoV2-N antibodies. For the regeneration of SCoV2-N/anti-SCoV2-N complex the solution containing 50 mM NaOH and 17.34 mM SDS was injected into the chamber for 5 min. After that, the chamber was filled with PBS pH 7.4 and the baseline was established. The effectiveness of regeneration was evaluated by

comparing the PBS baselines after a certain period of time from the start of experiment. As shown in Fig. 2, the baselines of PBS after SCoV2-N covalent immobilization (at 160 min) and after the regeneration of the surface (at 270 min) are at the same level. After regeneration of SCoV2-N/anti-SCoV2-N (anti-SCoV2-N was removed from the surface modified with SCoV2-N), the control solution containing the same concentration (170 nM) of nonspecific antibodies from non-immunized mice were injected for 30 min. In this case, no distinguishable change in SE or QCM-D signals was observed (Fig. 2, part 3). Finally, the chamber was washed with PBS. In this case, ΔF was 1.68 Hz and ΔD was $1.05 \cdot 10^{-6}$. Such a small ΔF showed that the interaction between SCoV2-N and the control solution containing non-specific antibodies was not established and the frequency change can be associated with non-specific adsorption of some proteins.

$\Delta D/\Delta F$ plots of QCM-D data were obtained by plotting ΔF (representing the increase in mass on the surface) on the x axis and ΔD (representing the changes in viscoelastic properties of the layer) on the y axis and eliminating time as an explicit parameter [32,33]. The $\Delta D/\Delta F$ plot is a complementary method of data presentation and it highlights the viscoelastic processes that occur during the protein monolayer formation [33]. The $\Delta D/\Delta F$ plots presented in Fig. 3 show how the viscoelastic properties change during the formation of the SCoV2-N monolayer and the subsequent interaction with anti-SCoV2-N, i.e. the formation of immune complexes.

During the covalent immobilization of SCoV2-N on the 11-MUA SAM, the increase in ΔD was gradual from the initial stage and consistent with the frequency change. The density of the points indicated the fast and slow steps of the SCoV2-N immobilization kinetics. As can be seen from curve 1 in Fig. 3, the points are more distantly placed when ΔF is from 0 to 25 Hz. This feature indicates
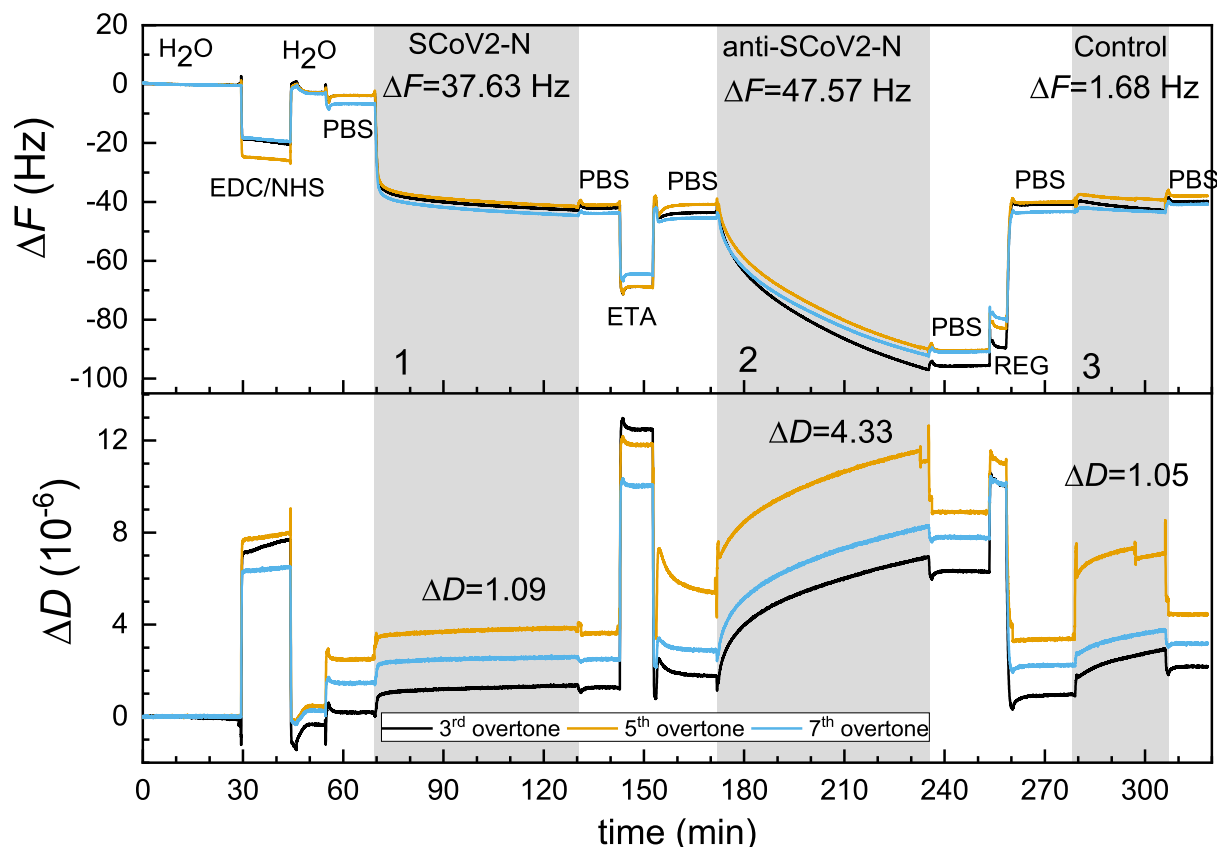

Fig. 2. Real-time frequency (ΔF) and energy dissipation (D) change for: (1) covalent SCoV2-N immobilization, (2) affinity interaction with anti-SCoV2-N, and (3) nonspecific interaction with polyclonal antibodies from mice non-immunized with SCoV2-N.
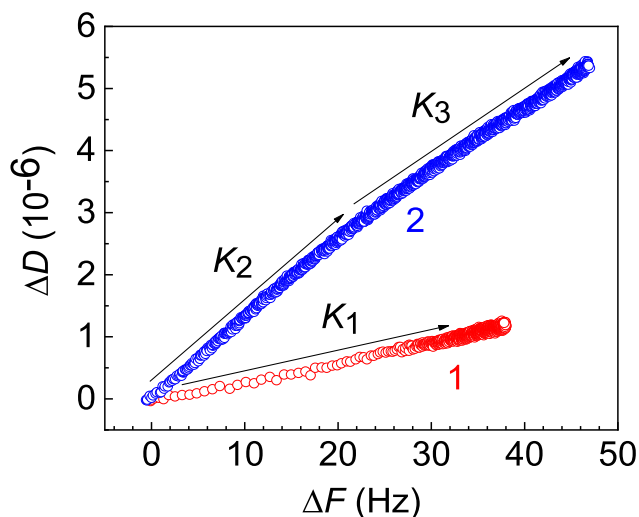
Fig. 3. $\Delta D/\Delta F$ plots for: SCoV2-N covalent immobilization on 11-MUA SAM (curve 1), and affinity interaction with anti-SCoV2-N (curve 2). The arrows K_1, K_2, and K_3 indicate the slopes to curves 1 and 2.

that in this particular ΔF range the kinetics of SCoV2-N covalent immobilization on 11-MUA SAM is faster than in the range from 25 to 38 Hz. The range from 0 to 25 Hz is obtained during the beginning of SCoV2-N monolayer formation. The slope of K_1 calculated for SCoV2-N covalent immobilization on 11-MUA SAM was equal to 0.031. Such a small value of K_1 also indicated that the formed SCoV2-N monolayer is rigid and, therefore, Sauerbrey equation can be very accurately applied for the calculation of surface mass density [34]. For the formation of the SCoV2-N/anti-SCoV2-N complex, the increase in ΔD was gradual from the beginning, with a slight change of direction in the $\Delta D/\Delta F$ plot at 22 Hz, thus curve 2 had two distinct tangents – K_2 and K_3 (Fig. 3, curve 2). This small change of SCoV2-N and anti-SCoV2-N interaction can be associated with conformational changes and rearrangements of anti-SCoV2-N antibodies during the formation of the SCoV2-N/anti-SCoV2-N complex [34]. The $\Delta D/\Delta F$ plot (Fig. 3, curve 2) shows that the formation of SCoV2-N/anti-SCoV2-N complex is slow because the points are distributed close to each other from the beginning of the interaction with SCoV2-N. The calculated slopes K_2 and K_3 for the formation of the SCoV2-N/anti-SCoV2-N complex were 0.134 and 0.121, respectively. These values are close to those obtained by other authors for cysteine peptidase and specific polyclonal antibody complex formation [34]. However, higher values of ΔD registered during anti-SCoV2-N affinity interaction with immobilized SCoV2-N show that the formation of the SCoV2-N/anti-SCoV2-N complex creates a soft and viscoelastic layer of anti-SCoV2-N antibodies. As it was reported in our previous publication [29], the equilibrium dissociation constant K_D of SCoV2-N/anti-SCoV2-N complex obtained from spectroscopic ellipsometry measurements in the total internal reflection mode was $9.3 \cdot 10^{-7}$ M (Table 1).

Most antibodies have K_D values are in the range of 10^{-6} to 10^{-9}. Antibody affinity can be measured using different methods such as label-free optical scanner for microarray detection based on polarization-modulated oblique-incidence reflectivity difference,

SPR, and ellipsometry-based (label-free) optical scanner [11,35–38]. K_D calculated from the experimental results obtained after polyclonal anti-SCoV2-N interaction with covalently immobilized SCoV2-N falls in this range of K_D values.

3.2. Analysis of SCoV2-N monolayer and SCoV2-N/anti-SCoV2-N complex formation by SE

For the evaluation of SCoV2-N covalent immobilization on 11-MUA SAM and SCoV2-N/anti-SCoV2-N complex formation on the gold-coated sensor disk, measurements of ellipsometric parameters (Δ and Ψ) were performed simultaneously with QCM-D signals registration (ΔF and ΔD). Here we present only the kinetics of the ellipsometric parameter Δ due to its higher sensitivity [16,22,39]. The simulation of ellipsometric parameters Ψ and Δ vs λ has been conducted to determine the difference between the optical properties in case of full coverage by SCoV2-N and anti-SCoV2-N versus partial coverage by the same proteins. Then the evaluation of fully formed SCoV2-N and anti-SCoV2-N monolayers was performed by the simulation of Δ and Ψ vs λ curves according to Cauchy dispersion function using Complete EASE software for ellipsometric data analysis.

The refractive index n of such fully formed monolayers in both cases (SCoV2-N and anti-SCoV2-N) was 1.6 at 600 nm wavelength. Measured and simulated Δ vs λ dispersion curves are presented for comparison in Fig. 4A for SCoV2-N, and Fig. 4B for anti-SCoV2-N, respectively. Curves 1 and 1′ presented in Fig. 4 A, and B correspond to the pure PBS (n = 1.333) before injection of SCoV2-N and before the SCoV2-N/anti-SCoV2-N complex formation. Curves 2 and 2′ were obtained experimentally when monolayers of SCoV2-N and anti-SCoV2-N antibodies were formed, respectively. The $\delta\Delta$ differences calculated at 601 nm between curves 1 and 2, 1′ and 2′ (Fig. 4A, and B) were 1.11° after SCoV2-N monolayer formation and 0.81° after anti-SCoV2-N affinity interaction with immobilized SCoV2-N, respectively. This difference was compared to that between curves 1 and 3, 1′ and 3′ that corresponded to simulated fully formed monolayers (n = 1.6) of SCoV2-N and anti-SCoV2-N. Simulated data (Fig. 4A, curves 1–3) for the formed SCoV2-N monolayer showed that the $\delta\Delta$ between PBS and the fully formed SCoV2-N layer would be 8.01°. For the fully formed anti-SCoV2-N monolayer, $\delta\Delta$ would be 6.78° (Fig. 4B curves 1–3). The kinetics of SCoV2-N covalent immobilization and affinity interaction with anti-SCoV2-N are presented in Fig. 4 C and D, respectively. The $\delta\Delta$ presented in Fig. 4 C, and D for SCoV2-N and anti-SCoV2-N meets the difference between curves 1 and 2, 1′ and 2′ in Fig. 4 A, and B. As can be seen from these Figures, the SCoV2-N covers only small part on the surface. Consequently, only a small amount of anti-SCoV2-N forms a complex with covalently immobilized SCoV2-N.

3.3. Wet and dry SCoV2-N and anti-SCoV2-N layers' surface mass density calculation from SE and QCM-D data

For the calculation of SCoV2-N monolayer thickness and index of refraction (n), modelling of the experimentally obtained ellipsometric parameters Ψ and Δ vs λ was done by designing an optical model. The experimental results obtained were fitted with optical model using Complete EASE software for ellipsometric data analy-

Table 1
Association, dissociation, residence time rate constants (k_a, k_d, k_r), equilibrium association and dissociation constants (K_A, K_D) for SCoV2-N/anti-SCoV2-N immune complex formation . adopted from [29]

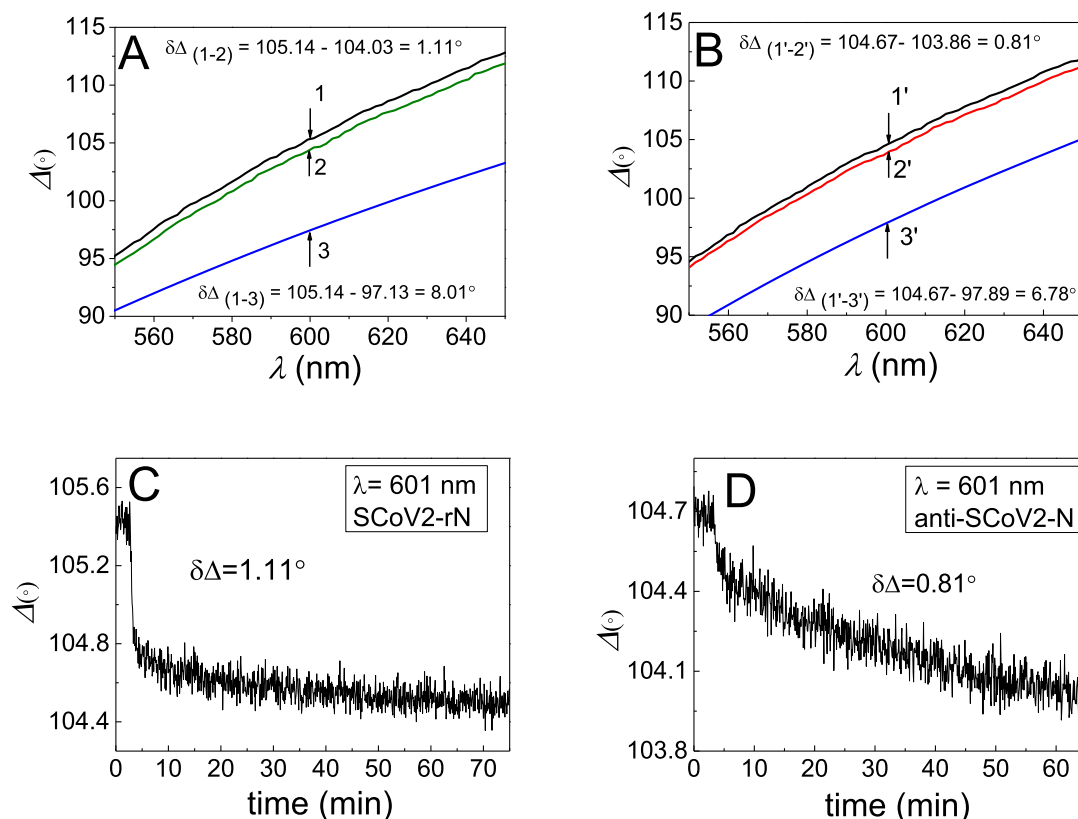|	k_a (M^{-1} s^{-1})	k_d (s^{-1})	K_A (M^{-1})	K_D (M)	k_r (s^{-1})
anti-SCoV2-N	$3.6 \cdot 10^4 \pm 0.002$	$3.35 \cdot 10^{-2} \pm 0.047$	$1.07 \cdot 10^6$	$9.3 \cdot 10^{-7}$	$4.8 \cdot 10^{-3} \pm 0.026$

Fig. 4. Spectra of ellipsometric parameter Δ vs. λ (**A, B**) and time (**C, D**) for covalent SCoV2-N immobilization and formation of immune complexes with specific anti-SCoV2-N antibodies. **A** - the ellipsometric parameter Δ vs λ for covalent SCoV2-N immobilization on 11-MUA SAM: 1- PBS, 2- SCoV2-N partially covered monolayer, 3- simulated monolayer fully covered by SCoV2-N; **B** - the ellipsometric parameter Δ vs. λ for SCoV2-N interaction with anti-SCoV2-N and monolayer formation: 1′- PBS, 2′- anti-SCoV2-N monolayer, 3′- simulated fully covered by anti-SCoV2-N; **C** - evolution of Δ in time for SCoV2-N covalent immobilization, and **D** – for anti-SCoV2-N monolayer formation.

sis. This model consisted of a thick QCM-D gold substrate, thickness $d_{(gold)}$ = 200 nm, covered by 11-MUA SAM, $d_{(SAM)}$ = 0.8 nm and $d_{(SCoV2-N)}$ = 5.9 nm SCoV2-N layers. The refractive index dispersion of the QCM-D gold-coated sensor substrate was modelled using B-Spline function [24], 11-MUA SAM was modelled by Cauchy dispersion (n = 1.450) and the SCoV2-N monolayer was described using the Bruggeman effective media approach (EMA) [22,39–41].

The monolayer of SCoV2-N described as EMA consisted of 66% PBS (n = 1.333) and of 34% SCoV2-N (n = 1.610). During the regression analysis for the calculation of the refractive index, the thickness of the monolayer $d_{(SCoV2-N)}$ was a fixed parameter and the volume fraction of PBS was a free fitting value in the EMA. The anti-SCoV2-N monolayer was fitted using the same Bruggeman EMA layer on top of SCoV2-N under the similar procedure. Anti-SCoV2-N monolayer consisted of 81% PBS and 19% of antibody, the thickness of this monolayer $d_{(anti- SCoV2- N)}$ = 8 nm was a fixed value during regression analysis for modelling of n evolution in time. After that the thickness $d_{(SCoV2-N)}$ and $d_{(anti-SCoV2-N)}$ evolution in time was performed fixing the refractive index values of fully formed SCoV2-N and anti-SCoV2-N monolayers (Fig. 5A, B). Anti-SCoV2-N $d_{(anti-SCoV2-N)}$ obtained from regression analysis of SE data was further fitted to be 8.1 nm and this value is close to one of the IgG antibody dimensions, when the antigen-binding sites are in about 13.7 nm distance [42]. This means that the conformation of anti-SCoV2-N antibodies on the surface of the formed SCoV2-N layer is T shape [43]. As the Ab is a flexible molecule and the mean angle between antibody Fab-Fab arms can differ, the T shape position makes it possible to reach small antigens located on the surface far from each other [44] and to establish a tightly bound

complex [45]. The calculated Δn, $d_{(SCoV2-N)}$ and $d_{(anti-SCoV2-N)}$ evolution in time for the formation of SCoV2-N and anti-SCoV2-N monolayers are presented in Fig. 5C, D. Calculation of dry layers thickness d and refractive index changes Δn from the results obtained by SE allowed us to evaluate the dry surface mass density for SCoV2-N and anti-SCoV2-N monolayers.

As shown in Fig. 5C, after 70 min, when the SCoV2-N monolayer was formed, the difference in refractive indexes $\Delta n = (n_{SCoV2-N} - n_{PBS})$ = 0.08. For anti-SCoV2-N, Δn = 0.38 after 70 min (Fig. 5D). Surface mass densities calculated using SE data (Γ^{SE}) of SCoV2-N or anti-SCoV2-N monolayers ($\Gamma^{SE}_{SCoV2-N}$ and $\Gamma^{SE}_{anti-SCoV2-N}$) presented in Fig. 5E, F were calculated using de Feijter approach:

$$\Gamma^{SE} = \frac{d(n_{layer} - n_{PBS})}{dn/dc} \cdot 100 \tag{1}$$

Here d is the thickness of the formed antigen or antibody monolayer (SCoV2-N or anti-SCoV2-N), dn/dc is the refractive index increment for proteins (0.18) [24,40,46]. The evolution of $\Gamma^{SE}_{SCoV2-N}$ and $\Gamma^{SE}_{anti-SCoV2-N}$ in time during monolayer formation is presented in Fig. 5E, and F. Γ^{SE} for the SCoV2-N and anti-SCoV2-N layers corresponds to the dry mass, without PBS between the proteins. Calculated dry mass Γ^{SE} for the SCoV2-N monolayer was 200 ng/cm^2 after 70 min and for anti-SCoV2-N (the initial concentration of specific antibodies was 170 nM) was 167 ng/cm^2.

When the SCoV2-N monolayer was formed (after 70 min), the wet surface mass density calculated using QCM-D data obtained simultaneously with SE was C = 672 ng/cm^2 (Fig. 5E). The Γ^{QCM-D} was calculated using Voinova-Voight model in the QSoft401 software (Biolin Scientific) [47,48]. After anti-SCoV2-N interaction
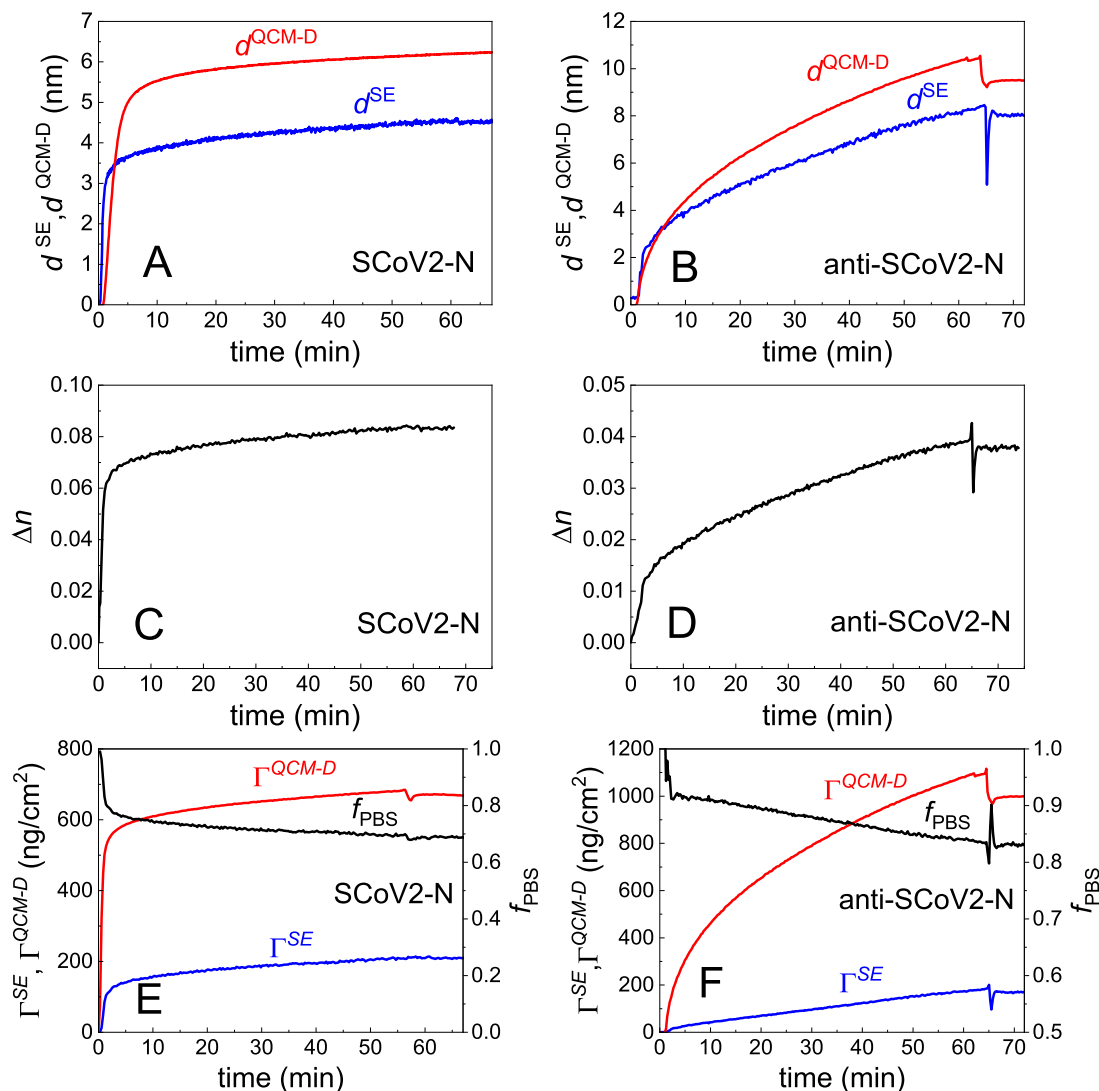
Fig. 5. Evolution of the formation of SCoV2-N and anti-SCoV2-N monolayers in time: dry (d^{SE}) and wet (d^{QCM-D}) monolayer thickness versus time for SCoV2-N (**A**) and anti-SCoV2-N (**B**), change of refractive index versus time for SCoV2-N (**C**) and anti-SCoV2-N (**D**), and dry (Γ^{SE}) and wet (Γ^{QCM-D}) surface mass density for SCoV2-N (**E**) and anti-SCoV2-N (**F**).

with immobilized SCoV2-N and anti-SCoV2-N monolayer formation (70 min), wet Γ^{QCM-D} = 995 ng/cm² (Fig. 5F). The Γ^{QCM-D} corresponds to the wet mass and presents the surface mass density for the monolayer containing SCoV2-N or anti-SCoV2-N molecules, and PBS. The thicknesses of the SCoV2-N and anti-SCoV2-N wet layers calculated from QCM-D data modelling were 6.24 nm and 9.55 nm, respectively. Calculated hydration (f_{PBS}) of the protein layers is presented in Fig. 5E and 5F as the amount of PBS trapped between the molecules of the SCoV2-N or anti-SCoV2-N.

Using SE in combination with QCM-D, changes in the amount of PBS between SCoV2-N and anti-SCoV2-N were evaluated simultaneously. The hydration was calculated using the following formula (2) [49]:

$$f_{PBS} = 1 - \frac{\Gamma^{SE}}{\Gamma^{QCM-D}} \qquad (2)$$

Here f_{PBS} is the amount of PBS between protein SCoV2-N or anti-SCoV2-N monolayers, Γ^{SE} - dry mass of SCoV2-N or anti-SCoV2-N, Γ^{QCM-D} – wet mass of SCoV2-N or anti-SCoV2-N + PBS. In this case, the amount of PBS in the SCoV2-N monolayer was close to 0.7 and for the anti-SCoV2-N monolayer the amount of PBS was 0.83

(Fig. 5E and F). These values of hydration (amount of PBS) for the SCoV2-N and anti-SCoV2-N monolayers are in good agreement with the results obtained from SE data modeling, where the amount of PBS in the SCoV2-N monolayer was 66% and for anti-SCoV2-N monolayer it was 81%, respectively.

Assuming that SCoV2-N monolayer is formed as a square shape site lattice and using simple geometrical considerations, it is possible to estimate the minimal distance between the SCoV2-N immobilized on the surface (lattice constant d_l) using the calculated hydration (f_{PBS}). Using such a geometrical model, d_l can be obtained from the formula $d_l = r \cdot (2\pi/3f)^{1/2}$, where r is the radius of the SCoV2-N molecule of ball-like shape. At r = 3 nm and f_{PBS} = 0.325, the d_l calculated using this formula was about 7.6 nm. Another way to estimate the d_l is to calculate the surface density of SCoV2-N molecules immobilized on the square unit (cm²) of the substrate. It can be done by dividing the total mass (m_{pt}) of these molecules by the mass (m_{ps} = 48 kDa) of a single SCoV2-N molecule ("mass" model). It should be noted that m_{pt} value depends on f_{PBS} and protein's density (ρ_p), which can be in the range of 1.22–1.34 g/cm³. For this reason, the surface density of the square-shaped site lattice changes from 3.0 10¹² cm⁻² to 3.3 10¹² cm⁻² and d_l ranged from 6.0 to 5.5 nm correspondingly, which is of the same order as obtained
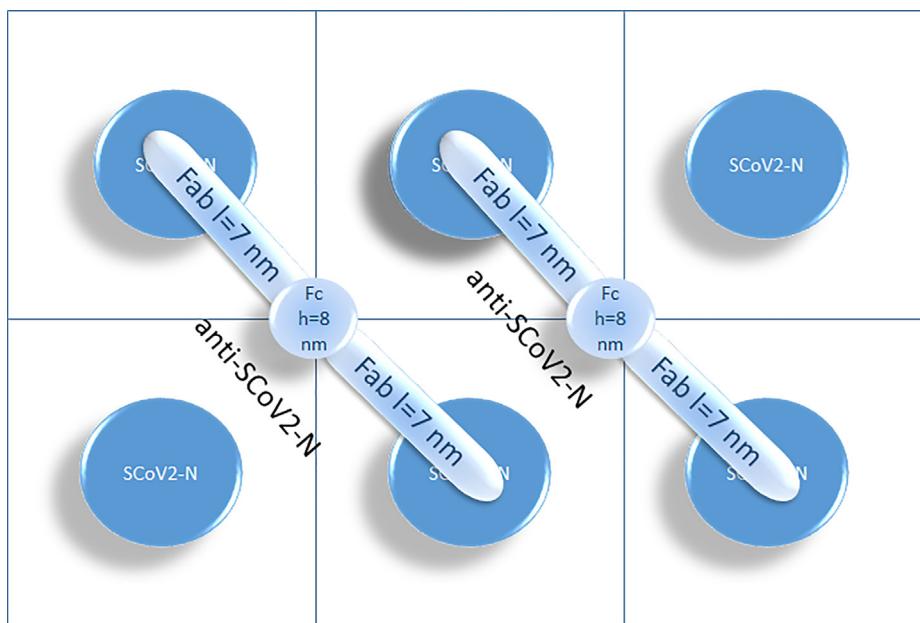
Fig. 6. Schematic representation (the relative sizes of SCoV2-N and anti-SCoV2-N are not in scale) of the displacement of SCoV2-N approximated by a square lattice. The lattice constant is the average distance between SCoV2-N molecules of the real monolayer.

from the geometrical model. The difference in about 20% of d_l value estimated using both "mass" and geometrical models can be easy explained taking into consideration that "mass" model assume hard packaging of protein material into one SCoV2-N molecule, meanwhile the geometrical model, which is more close to reality, is based on soft larger size molecule approach.

Assuming that SCoV2-N monolayer is formed as a square shape site lattice and using simple geometrical considerations, it is possible to estimate the minimal distance between the SCoV2-N immobilized on the surface (lattice constant d_l) using the calculated f_{PBS}. The d_l can be obtained from the formula $d_l = r \cdot (2\pi/3f)^{1/2}$, where r is the radius of the ball-shaped SCoV2-N molecule. At $r = 3$ nm and $f = 0.3$, the d_l calculated using this formula was 7.9 nm. The other important parameter of such a lattice is the diagonal distance (d_d) between the middle of each SCoV2-N molecules, that is, $d_d = d_l \cdot 2^{1/2} = 11.2$ nm. Thus, there are two possible ways to attach anti-SCoV2-N to the SCoV2-N using d_l and d_d distances. It is evident that d_d is preferable because in this case the anti-SCoV2-N present in T shape and a distance between the middle of each SCoV2-N molecules is close to 14 nm distance between paratopes. To evaluate the maximal hydration of the formed monolayer after affinity interaction of SCoV2-N with anti-SCoV2-N, we used the approximated square lattice presented in Fig. 6.

As can be seen, the lattice unit is occupied by one SCoV2-N molecule, one anti-SCoV2-N Fab fragment, and half of the anti-SCoV2-N Fc unit (two quarters of Fc fragments from two anti-SCoV2-N). Taking into account that the radius of SCoV2-N is 3 nm and the density of both proteins, i.e. SCoV2-N and anti-SCoV2-N is the same, we estimated that the diameter of the average anti-SCoV2-N cross section is about 2 nm. Thus, the total volume occupied by the proteins in one lattice unit (V_{pr}) consisting of SCoV2-N, an anti-SCoV2-N Fab fragment, and half of anti-SCoV2-N Fc fragment is approximately $V_{pr} = 434$ nm^3. The volume of a lattice unit (V_l) $7.9 \times 7.9 \times 14$ nm^3 is approximately $V_l = 874$-nm^3. The height of this lattice unit, i.e., 14 nm, was estimated as a sum of SCoV2-N monolayer thickness (6 nm) and anti-SCoV2-N monolayer thickness (8 nm). Thus, the maximal hydration of the formed SCoV2-N/anti-SCoV2-N complex $f_{comp} = V_{pr}/V_l \approx 0.5$. This value is close to $f_{comp} = 0.47$ obtained from hydration calculations

for SCoV2-N/anti-SCoV2-N (for SCoV2-N $f_{comp} = 0.3$ (Fig. 5E) and for anti-SCoV2-N $f_{comp} = 0.17$ (Fig. 5F), respectively).

4. Conclusions

SARS-CoV-2 nucleocapsid protein is one of the diagnostic markers that can be detected earlier than the clinical symptoms appears in infected patients [50]. Conversely, the detection of specific antibodies against nucleocapsid protein can increase the diagnostic capacity [51,52]. Based on our results we showed that the monolayer formed on the solid–liquid interface as a result of covalent immobilization of SCoV2-N can be described as a rigid due to low energy dissipation registered during QCM-D measurement. In contrary, anti-SCoV2-N monolayer after the interaction with the covalently immobilized SCoV2-N formed a soft, flexible, and viscous layer with 3.9 times higher energy dissipation. The flexibility of the antibody Fab arms allows them to reach the more distantly located SCoV2-N and to establish a bivalent interaction between proteins in formed SCoV2-N/anti-SCoV2-N complex. Different methods, such as electron microscopy [8], cryo-electron tomography [53], small-angle X-ray scattering [49], and other techniques were used to evaluate the flexibility of antibodies and conformational variability of the antigen-binding fragments. In this research we showed that SE/QCM-D can be applied for the evaluation of antibody flexibility and for the selection of antibodies with the desired properties since this factor limits the assembly of antibodies on the surface with immobilized antigens. The antibody flexibility can be taken into account for the design of sensitive immunoassays of different formats whereas distinct types of immune complexes (closed sandwich-like or the extended linear complexes of antibodies and antigens) can be formed. It was showed that in the direct sandwich enzyme-linked immunosorbent assay, the rigid enzyme-labeled antibody with dominating linear arrangement increased the sensitivity of the analytical system while more labeled antibody was bound to the same surface concentration of antigen in comparison to the flexible enzyme-labeled antibodies [50].

All in all, we have applied and adapted the combination of two highly surface-sensitive and label-free methods, that enables

simultaneously to study interaction between novel coronavirus SARS-CoV-2 nucleocapsid protein and specific antibody at the solid–liquid interface in real time and to evaluate viscoelastic properties of formed layers. The obtained results showed that anti-SCoV2-N flexibility was important factor for the bivalent interaction with small nucleocapsid protein distantly located from each other on the solid–liquid interface.

CRediT authorship contribution statement

Ieva Plikusiene: Conceptualization, Methodology, Visualization, Investigation, Writing – review & editing, Formal analysis, Writing – original draft. **Vincentas Maciulis:** Methodology, Formal analysis, Investigation, Writing – original draft. **Silvija Juciute:** Methodology, Investigation. **Arunas Ramanavicius:** Conceptualization, Methodology, Writing – review & editing. **Zigmas Balevicius:** Methodology, Conceptualization, Writing – review & editing. **Rimantas Slibinskas:** Methodology, Writing – original draft, Resources. **Indre Kucinskaite-Kodze:** Methodology, Resources. **Martynas Simanavicius:** Methodology, Resources. **Saulius Balevicius:** Methodology, Writing – review & editing, Formal analysis, Writing – original draft. **Almira Ramanaviciene:** Conceptualization, Visualization, Writing – original draft, Writing – review & editing, Funding acquisition, Supervision.

Declaration of Competing Interest

The authors declare that they have no known competing financial interests or personal relationships that could have appeared to influence the work reported in this paper.

Acknowledgment

References

[1] P.S. Masters, Coronavirus genomic RNA packaging, Virology 537 (2019) 198–207, https://doi.org/10.1016/j.virol.2019.08.031.
[2] M. Batra, R. Tian, C. Zhang, E. Clarence, C.S. Sacher, J.N. Miranda, J.R.O. De La Fuente, M. Mathew, D. Green, S. Patel, M.V.P. Bastidas, S. Haddadi, M. Murthi, M.S. Gonzalez, S. Kambali, K.H.M. Santos, H. Asif, F. Modarresi, M. Faghihi, M. Mirsaeidi, Role of IgG against N-protein of SARS-CoV2 in COVID19 clinical outcomes, Sci. Rep. 11 (2021) 1–9, https://doi.org/10.1038/s41598-021-83108-0.
[3] G. Guglielmi, Fast coronavirus tests: what they can and can't do, Nature 585 (2020) 496–498, https://doi.org/10.1038/d41586-020-02661-2.
[4] M. Drobysh, A. Ramanaviciene, R. Viter, A. Ramanavicius, Affinity sensors for the diagnosis of covid-19, Micromachines 12 (2021) 1–19, https://doi.org/10.3390/mi12040390.
[5] K. Guevara-Hoyer, J. Fuentes-Antrás, E. De la Fuente-Muñoz, A.R. de la Peña, M. Viñuela, N. Cabello-Clotet, V. Estrada, E. Culebras, A. Delgado-Iribarren, M. Martínez-Novillo, M.J. Torrejón, R.P. de Diego, M. Fernández-Arquero, A. Ocaña, P. Pérez-Segura, S. Sánchez-Ramón, Serological tests in the detection of SARS-CoV-2 antibodies, Diagnostics. 11 (2021) 1–10, https://doi.org/10.3390/diagnostics11040678.
[6] C. Dobaño, R. Santano, A. Jiménez, M. Vidal, J. Chi, N. Rodrigo Melero, M. Popovic, R. López-Aladid, L. Fernández-Barat, M. Tortajada, F. Carmona-Torre, G. Reina, A. Torres, A. Mayor, C. Carolis, A.L. García-Basteiro, R. Aguilar, G. Moncunill, L. Izquierdo, Immunogenicity and crossreactivity of antibodies to the nucleocapsid protein of SARS-CoV-2: utility and limitations in seroprevalence and immunity studies, Transl. Res. 232 (2021) 60–74. https://doi.org/10.1016/j.trsl.2021.02.006.
[7] P.D. Burbelo, F.X. Riedo, C. Morishima, S. Rawlings, D. Smith, S. Das, J.R. Strich, D.S. Chertow, R.T. Davey, J.I. Cohen, Sensitivity in detection of antibodies to nucleocapsid and spike proteins of severe acute respiratory syndrome coronavirus 2 in patients with coronavirus disease 2019, J. Infect. Dis. 222 (2020) 206–213, https://doi.org/10.1093/infdis/jiaa273.
[8] K.H. Roux, L. Strelets, T.E. Michaelsen, Flexibility of human IgG subclasses, J. Immunol. 159 (1997) 3372–3382. http://www.ncbi.nlm.nih.gov/pubmed/9317136.
[9] I.S. Mian, A.R. Bradwell, A.J. Olson, Structure, function and properties of antibody binding sites, J. Mol. Biol. 217 (1991) 133–151, https://doi.org/10.1016/0022-2836(91)90617-F.
[10] P. Wang, X. Yang, Neutralization Efficiency Is Greatly Enhanced by Bivalent Binding of an Antibody to Epitopes in the V4 Region and the Membrane-Proximal External Region within One Trimer of Human Immunodeficiency Virus Type 1 Glycoproteins, J. Virol. 84 (2010) 7114–7123, https://doi.org/10.1128/jvi.00545-10.
[11] L. Bar, J. Dejeu, R. Lartia, F. Bano, R.P. Richter, L. Coche-Guerente, D. Boturyn, Impact of Antigen Density on Recognition by Monoclonal Antibodies, Anal. Chem. 92 (2020) 5396–5403, https://doi.org/10.1021/acs.analchem.0c00092.
[12] K.B. Rodenhausen, B.A. Duensing, T. Kasputis, A.K. Pannier, T. Hofmann, M. Schubert, T.E. Tiwald, M. Solinsky, M. Wagner, In-situ monitoring of alkanethiol self-assembled monolayer chemisorption with combined spectroscopic ellipsometry and quartz crystal microbalance techniques, Thin Solid Films 519 (2011) 2817–2820, https://doi.org/10.1016/j.tsf.2010.11.081.
[13] J. Martensson, H. Arwin, Interpretation of Spectroscopic Ellipsometry Data on Protein Layers on Gold Including Substrate-Layer Interactions, Langmuir. 11 (1995) 963–968, https://doi.org/10.1021/la00003a045.
[14] H. Arwin, D.E. Aspnes, Unambiguous determination of thickness and dielectric function of thin films by spectroscopic ellipsometry, Thin Solid Films 113 (1984) 101–113, https://doi.org/10.1016/0040-6090(84)90019-1.
[15] H. Arwin, Spectroscopic ellipsometry and biology: Recent developments and challenges, Thin Solid Films 313–314 (1998) 764–774, https://doi.org/10.1016/S0040-6090(97)00993-0.
[16] H. Arwin, M. Poksinski, K. Johansen, Total internal reflection ellipsometry: Principles and applications, Appl. Opt. 43 (2004) 3028–3036, https://doi.org/10.1364/AO.43.003028.
[17] A.V. Nabok, A. Tsargorodskaya, A.K. Hassan, N.F. Starodub, Total internal reflection ellipsometry and SPR detection of low molecular weight environmental toxins, Appl. Surf. Sci. 246 (2005) 381–386, https://doi.org/10.1016/j.apsusc.2004.11.084.
[18] Z. Balevicius, A. Ramanaviciene, I. Baleviciute, A. Makaraviciute, L. Mikoliunaite, A. Ramanavicius, Evaluation of intact- and fragmented-antibody based immunosensors by total internal reflection ellipsometry, Sensors Actuat. B Chem. 160 (2011) 555–562, https://doi.org/10.1016/j.snb.2011.08.029.
[19] I. Baleviciute, Z. Balevicius, A. Makaraviciute, A. Ramanaviciene, A. Ramanavicius, Study of antibody/antigen binding kinetics by total internal reflection ellipsometry, Biosens. Bioelectron. 39 (2013) 170–176, https://doi.org/10.1016/j.bios.2012.07.017.
[20] Z. Balevicius, I. Baleviciute, S. Tumenas, L. Tamosaitis, A. Stirke, A. Makaraviciute, A. Ramanaviciene, A. Ramanavicius, In situ study of ligand-receptor interaction by total internal reflection ellipsometry, Thin Solid Films 571 (2014) 744–748, https://doi.org/10.1016/j.tsf.2013.10.090.
[21] Z. Balevicius, J. Talbot, L. Tamosaitis, I. Plikusiene, A. Stirke, G. Mickiene, S. Balevicius, A. Paulauskas, A. Ramanavicius, Modelling of immunosensor response: the evaluation of binding kinetics between an immobilized receptor and structurally-different genetically engineered ligands, Sensors Actuat. B Chem. 297 (2019), https://doi.org/10.1016/j.snb.2019.126770 126770.
[22] I. Plikusiene, Z. Balevicius, A. Ramanaviciene, J. Talbot, G. Mickiene, S. Balevicius, A. Stirke, A. Tereshchenko, L. Tamosaitis, G. Zvirblis, A. Ramanavicius, Evaluation of affinity sensor response kinetics towards dimeric ligands linked with spacers of different rigidity: Immobilized recombinant granulocyte colony-stimulating factor based synthetic receptor binding with genetically engineered dimeric analyte d, Biosens. Bioelectron. 156 (2020), https://doi.org/10.1016/j.bios.2020.112112 112112.
[23] I. Plikusiene, V. Maciulis, S. Juciute, R. Maciuleviciene, S. Balevicius, A. Ramanavicius, A. Ramanaviciene, Investigation and Comparison of Specific Antibodies' Affinity Interaction with SARS-CoV-2 Wild-Type, B.1.1.7, and B.1.351 Spike Protein by Total Internal Reflection Ellipsometry, Biosensors. 12 (2022) 351, https://doi.org/10.3390/bios12050351.
[24] E. Bittrich, K.B. Rodenhausen, K.-J. Eichhorn, T. Hofmann, M. Schubert, M. Stamm, P. Uhlmann, Protein adsorption on and swelling of polyelectrolyte brushes: A simultaneous ellipsometry-quartz crystal microbalance study, Biointerphases. 5 (2010) 159–167, https://doi.org/10.1116/1.3530841.
[25] H.T.M. Phan, S. Bartelt-Hunt, K.B. Rodenhausen, M. Schubert, J.C. Bartz, D. Hinderberger, Investigation of bovine serum albumin (BSA) attachment onto self-assembled monolayers (SAMs) using combinatorial quartz crystal microbalance with dissipation (QCM-D) and spectroscopic ellipsometry (SE), PLoS One 10 (10) (2015) e0141282.
[26] M.V. Voinova, M. Rodahl, M. Jonson, B. Kasemo, Viscoelastic acoustic response of layered polymer films at fluid-solid interfaces: continuum mechanics approach, Phys. Scr. 59 (1999) 391–396, https://doi.org/10.1238/physica.regular.059a00391.
[27] M.B. Hovgaard, K. Rechendorff, J. Chevallier, M. Foss, F. Besenbacher, Fibronectin adsorption on tantalum: The influence of nanoroughness, J. Phys. Chem. B. 112 (2008) 8241–8249, https://doi.org/10.1021/jp801103n.
[28] S. Adam, M. Koenig, K.B. Rodenhausen, K.J. Eichhorn, U. Oertel, M. Schubert, M. Stamm, P. Uhlmann, Quartz crystal microbalance with coupled spectroscopic

ellipsometry-study of temperature-responsive polymer brush systems, Appl. Surf. Sci. 421 (2017) 843–851, https://doi.org/10.1016/j.apsusc.2017.02.078.

[29] I. Plikusiene, V. Maciulis, A. Ramanaviciene, Z. Balevicius, E. Buzavaite-Verteliene, E. Ciplys, R. Slibinskas, M. Simanavicius, A. Zvirbliene, A. Ramanavicius, Evaluation of kinetics and thermodynamics of interaction between immobilized SARS-CoV-2 nucleoprotein and specific antibodies by total internal reflection ellipsometry, J. Colloid Interface Sci. 594 (2021) 195–203, https://doi.org/10.1016/j.jcis.2021.02.100.

[30] P. Hampitak, D. Melendrez, M. Iliut, M. Fresquet, N. Parsons, B. Spencer, T.A. Jowitt, A. Vijayaraghavan, Protein interactions and conformations on graphene-based materials mapped using quartz-crystal microbalance with dissipation monitoring (QCM-D), Carbon N. Y. 165 (2020) 317–327, https://doi.org/10.1016/j.carbon.2020.04.093.

[31] G. Sauerbrey, Verwendung von Schwingquarzen zur Wägung dünner Schichten und zur Mikrowägung, Zeitschrift Für Phys. 155 (1959) 206–222, https://doi.org/10.1007/BF01337937.

[32] F. Höök, M. Rodahl, B. Kasemo, P. Brzezinski, Structural changes in hemoglobin during adsorption to solid surfaces: Effects of pH, ionic strength, and ligand binding, Proc. Natl. Acad. Sci. USA 95 (1998) 12271–12276, https://doi.org/10.1073/pnas.95.21.12271.

[33] A. Makaraviciute, T. Ruzgas, A. Ramanavicius, A. Ramanaviciene, Antibody fragment immobilization on planar gold and gold nanoparticle modified quartz crystal microbalance with dissipation sensor surfaces for immunosensor applications, Anal. Methods 6 (2014) 2134–2140, https://doi.org/10.1039/c4ay00070f.

[34] A.S. Afonso, B.F. Zanetti, A.C. Santiago, F. Henrique-Silva, L.H.C. Mattoso, R.C. Faria, QCM immunoassay for recombinant cysteine peptidase: A potential protein biomarker for diagnosis of citrus canker, Talanta 104 (2013) 193–197, https://doi.org/10.1016/j.talanta.2012.11.003.

[35] J.P. Landry, Y. Fei, X. Zhu, Simultaneous measurement of 10,000 protein-ligand affinity constants using microarray-based kinetic constant assays, Assay Drug Dev. Technol. 10 (2012) 250–259, https://doi.org/10.1089/adt.2011.0406.

[36] Y. Fei, Y.S. Sun, Y. Li, K. Lau, H. Yu, H.A. Chokhawala, S. Huang, J.P. Landry, X. Chen, X. Zhu, Fluorescent labeling agents change binding profiles of glycan-binding proteins, Mol. Biosyst. 7 (2011) 3343–3352, https://doi.org/10.1039/c1mb05332a.

[37] Y.S. Sun, J.P. Landry, Y.Y. Fei, X.D. Zhu, J.T. Luo, X.B. Wang, K.S. Lam, Effect of fluorescently labeling protein probes on kinetics of protein-ligand reactions, Langmuir. 24 (2008) 13399–13405, https://doi.org/10.1021/la802097z.

[38] D.G. Myszka, M.D. Jonsen, B.J. Graves, Equilibrium analysis of high affinity interactions using BIACORE, Anal. Biochem. 265 (1998) 326–330, https://doi.org/10.1006/abio.1998.2937.

[39] I. Plikusiene, V. Maciulis, O. Graniel, M. Bechelany, S. Balevicius, V. Vertelis, Z. Balevicius, A. Popov, A. Ramanavicius, A. Ramanaviciene, Total internal reflection ellipsometry for kinetics-based assessment of bovine serum albumin immobilization on ZnO nanowires, J. Mater. Chem. C 9 (2021) 1345–1352, https://doi.org/10.1039/d0tc05193d.

[40] Z. Balevicius, A. Paulauskas, I. Plikusiene, L. Mikoliunaite, M. Bechelany, A. Popov, A. Ramanavicius, A. Ramanaviciene, Towards the application of Al2O3/ZnO nanolaminates in immunosensors: total internal reflection spectroscopic ellipsometry based evaluation of BSA immobilization, J. Mater. Chem. C 6 (2018) 8778–8783, https://doi.org/10.1039/c8tc03091j.

[41] V. Maciulis, U. Malinovskis, D. Erts, A. Ramanavicius, A. Ramanaviciene, S. Balevicius, S. Juciute, I. Plikusiene, Porous aluminium oxide coating for the development of spectroscopic ellipsometry based biosensor: Evaluation of human serum albumin adsorption, Coatings 10 (2020) 1–10, https://doi.org/10.3390/coatings10111018.

[42] Y.H. Tan, M. Liu, B. Nolting, J.G. Go, J. Gervay-hague, G. Liu, ARTICLE A nanoengineering approach for immobilization, ACS Nano 2 (2008) 2374–2384.

[43] H.R. Maun, R. Vij, B.T. Walters, A. Morando, J.K. Jackman, P. Wu, A. Estevez, X. Chen, Y. Franke, M.T. Lipari, M.S. Dennis, D. Kirchhofer, C. Ciferri, K.M. Loyet, T. Yi, C. Eigenbrot, R.A. Lazarus, J.T. Koerber, Bivalent antibody pliers inhibit β-tryptase by an allosteric mechanism dependent on the IgG hinge, Nat. Commun. 11 (2020) 1–12, https://doi.org/10.1038/s41467-020-20143-x.

[44] S. Sandin, L.G. Öfverstedt, A.C. Wikström, Ö. Wrange, U. Skoglund, Structure and flexibility of individual immunoglobulin G molecules in solution, Structure. 12 (2004) 409–415, https://doi.org/10.1016/j.str.2004.02.011.

[45] I. Correia, J. Sung, R. Burton, C.G. Jakob, B. Carragher, T. Ghayur, C. Radziejewski, The structure of dual-variable-domain immunoglobulin molecules alone and bound to antigen, MAbs. 5 (2013) 364–372, https://doi.org/10.4161/mabs.24258.

[46] H. Zhao, P.H. Brown, P. Schuck, On the distribution of protein refractive index increments, Biophys. J. 100 (2011) 2309–2317, https://doi.org/10.1016/j.bpj.2011.03.004.

[47] M.V. Voinova, M. Jonson, B. Kasemo, Dynamics of viscous amphiphilic films supported by elastic solid substrates, J. Phys. Condens. Matter. 9 (1997) 7799–7808, https://doi.org/10.1088/0953-8984/9/37/011.

[48] M.V. Voinova, M. Jonson, B. Kasemo, "Missing mass" effect in biosensor's QCM applications, Biosens. Bioelectron. 17 (2002) 835–841, https://doi.org/10.1016/S0956-5663(02)00050-7.

[49] K.B. Rodenhausen, M. Schubert, Virtual separation approach to study porous ultra-thin films by combined spectroscopic ellipsometry and quartz crystal microbalance methods, Thin Solid Films 519 (2011) 2772–2776, https://doi.org/10.1016/j.tsf.2010.11.079.

[50] C.D. Hodge, D.J. Rosenberg, P. Grob, M. Wilamowski, A. Joachimiak, G.L. Hura, M. Hammel, C.D. Hodge, D.J. Rosenberg, P. Grob, M. Wilamowski, A. Joachimiak, G.L. Hura, M. Hammel, Rigid monoclonal antibodies improve detection of SARS-CoV-2 nucleocapsid protein ABSTRACT, MAbs 13 (2021), https://doi.org/10.1080/19420862.2021.1905978.

[51] D.L. Ng, G.M. Goldgof, B.R. Shy, A.G. Levine, J. Balcerek, S.P. Bapat, J. Prostko, M. Rodgers, K. Coller, S. Pearce, S. Franz, L. Du, M. Stone, S.K. Pillai, A. Sotomayor-Gonzalez, V. Servellita, C.S.S. Martin, A. Granados, D.R. Glasner, L.M. Han, K. Truong, N. Akagi, D.N. Nguyen, N.M. Neumann, D. Qazi, E. Hsu, W. Gu, Y.A. Santos, B. Custer, V. Green, P. Williamson, N.K. Hills, C.M. Lu, J.D. Whitman, S.L. Stramer, C. Wang, K. Reyes, J.M.C. Hakim, K. Sujishi, F. Alazzeh, L. Pham, E. Thornborrow, C.-Y. Oon, S. Miller, T. Kurtz, G. Simmons, J. Hackett, M.P. Busch, C.Y. Chiu, SARS-CoV-2 seroprevalence and neutralizing activity in donor and patient blood, Nat. Commun. 11 (2020) 4698, https://doi.org/10.1038/s41467-020-18468-8.

[52] L. Wanbing, L. Lei, K. Guomei, Z. Yaqiong, D. Yinjuan, N. Wenxu, W. Qiongshu, T. Li, W. Wanlei, T. Shi, X. Zhou, Z. Shangen, M.a. j.,, Evaluation of Nucleocapsid and Spike Protein-Based Enzyme-Linked Immunosorbent Assays for Detecting Antibodies against SARS-CoV-2, J. Clin. Microbiol. 58 (2022) e00461–e520, https://doi.org/10.1128/JCM.00461-20.

[53] L. Bongini, D. Fanelli, F. Piazza, P.D.L. Rios, S. Sandin, U. Skoglund, Dynamics of antibodies from cryo-electron tomography, 115 (2005) 235–240. https://doi.org/10.1016/j.bpc.2004.12.037.